Creep rupture limit analysis for engineering structures under high-temperature conditions

Xiaoxiao Wang[1], Zhiyuan Ma[1], Haofeng Chen[1,2*], Yinghua Liu[3], Duoqi Shi[4], Jie Yang[5]
[1]Department of Mechanical & Aerospace Engineering, University of Strathclyde, James Weir Building, 75 Montrose Street, Glasgow G1 1XJ, UK
[2]School of Mechanical and Power Engineering, East China University of Science and Technology, Shanghai 200237, China
[3]Department of Engineering Mechanics, Tsinghua University, Beijing 100084, China
[4]School of Energy and Power Engineering, Beihang University, Beijing 100191, China
[5]School of Energy and Power Engineering, University of Shanghai for Science and Technology, Shanghai 200093, China

ABSTRACT

The efficient and accurate prediction of creep rupture limit poses a huge challenge for high-temperature engineering such as aerospace, nuclear and chemical industries. It is important to investigate the applicability of mainstream assessment approaches and related creep rupture failure mechanisms through theoretical and numerical views. In this study, major creep rupture assessment techniques are comparatively investigated for the first time, including the isochronous stress-strain (ISS) curve-based creep rupture limit analysis, the Omega creep damage model-based creep analysis and the direct method-based creep rupture assessment by an extended Linear Matching Method (LMM). New virtual creep test curves are generated from the Omega creep model and chosen as the unified creep source data to derive the key material parameters used for different methods. For proposing a reasonable strategy for evaluating high-temperature structures in terms of creep rupture, the balance between computational efficiency and accuracy is comprehensively analyzed. Through a practical engineering application of a high-temperature pressure vessel component, a profound insight into the techniques of creep rupture evaluation is delivered from different views. Moreover, several assessment curves are built based on a new

This is a peer-reviewed, accepted author manuscript of the following article: Wang, X., Ma, Z., Chen, H., Liu, Y., Shi, D., & Yang, J. (Accepted/In press). Creep rupture limit analysis for engineering structures under high-temperature conditions. International Journal of Pressure Vessels and Piping.

understanding of creep rupture failure mechanism, with an effective numerical plan to validate the creep rupture boundary illustrated. It is demonstrated that the LMM direct creep rupture analysis is more suitable for calculating the structural creep rupture limit, with both monotonic and cyclic load conditions considered.

Keywords: Creep rupture, LMM, Damage model, Isochronous stress-strain curve

Nomenclature

Abbreviations

CDM	continuum damage mechanics
EPP	elastic-perfectly plastic
FEA	finite element analysis
ISS	isochronous stress-strain
LMM	linear matching method
MPC	Material Properties Council
SDV	solution dependent state variables
XFEM	extended finite element method
3D	three-dimensional

Variables

A_i	creep date of strain rate parameter
B_i	creep date of Omega parameter
ε_{total}	total strain
$\varepsilon_{elastic}$	elastic strain
$\varepsilon_{plastic}$	plastic strain
ε_{creep}	creep strain
$\Delta\varepsilon_{ij}^{c}$	compatible strain increment over a cycle
$\Delta\varepsilon_{ij}^{new'}$	deviatoric component of new compatible strain increment
$\dot{\varepsilon}$	creep strain rate
$\dot{\varepsilon}_{oc}$	initial creep strain rate at the start of the time period being evaluated based on the stress state and temperature
$\dot{\varepsilon}_{ij}^{c}$	kinematically admissible strain rate
$\bar{\dot{\varepsilon}}$	effective strain rate
$\dot{\varepsilon}_{ij}^{new'}$	deviatoric component of new strain rate history in the next cycle
$\dot{\varepsilon}_{kk}^{new}$	hydrostatic component of the new strain rate history in the next cycle
$\bar{\dot{\varepsilon}}^{i}$	effective strain rate
σ_e	equivalent effective stress
$\hat{\sigma}_{ij}$	linear elastic stress field solution
σ_{ij}^{c}	stress yield at yield associated with $\dot{\varepsilon}_{ij}^{c}$
$\sigma_{ij}^{'in}$	deviatoric component of initial stress condition
$\hat{\sigma}_{ij}^{'}$	deviatoric component of linear elastic solution
σ_y	revised yield stress, MPa
σ_r	creep rupture stress, MPa
σ_s	material's yield stress, MPa
p	hydrostatic pressure stress
$\bar{\rho}_{ij}^{new}$	constant residual stress field
$\bar{\rho}'^{f}_{ij}$	deviatoric component of constant residual stress field

t	creep time, hours
t_r	creep rupture time, hours
t_{rA}	creep failure time for verification, hours
t_{rB}	creep failure time for verification, hours
Δt	period during the load cycle
m	Norton's exponent to describe the rate increase because of the cross-section reduction effect
p	microstructural damage
c	deficiencies in Norton's exponent and other microstructural factors related to the stress change
λ	load parameter
λ_{UB_LIMIT}	upper bound load parameter
$\lambda^{i}_{UB\_LIMIT}$	load parameter
$\lambda^{new}_{UB\_LIMIT}$	new upper bound load parameter
μ	matching condition parameter
$\bar{\mu}$	average of matching condition parameter over a cycle
μ_n	matching condition parameter during a cycle
D_c	creep damage variable
$\dot{D}_C$	creep damage rate
T	temperature, °C
E	Young's modulus, GPa
ν	Poisson's ratio
Ω	Omega parameters used in Omega creep model

1. Introduction

With the modern industrial equipment expecting higher temperature and pressure design requirements, the problems of how to prevent creep rupture failure, the crucial failure mode when the equipment works in this harsh environment, and how to make this design or assessment more efficient and accurate have been focused on for a long time [1]. Considering that the equipment running under high-temperature conditions often has an expensive cost and will produce huge security risks and economic losses after failure [2, 3], various design and assessment procedures against creep rupture behaviour have been developed by both industry and researchers.

As a widely used simplified creep rupture calculation, the isochronous strain stress (ISS) curve has been seen as a powerful and concise tool to evaluate the structural creep behaviour [4, 5], and it has been incorporated into ASME Boiler & Pressure Vessel Code Section III (including the Code Case) offering ISS curves for the majority of materials suitable for high-temperature engineering components(in Division 1, Subsection NH) [6, 7]. The origins and background of the ISS curve were described in detail by Douglas L. Marriott [4]. Although it is criticised for lacking sufficient theoretical support, the ISS curve method is still chosen as a kind of engineering alternative to viscoplastic finite element analysis (FEA) during creep assessment [8] since, for engineering application, it is not necessary to fully understand the complex creep damage mechanism behind these curves. It was reported that in many cases, the creep prediction by using ISS curve parameters could obtain reliable and acceptable approximate results, compared to others by FEA considering detailed material's creep constitutive modes, analytical solutions, and experiment results [9-13].

Another plan to implement creep prediction is to make use of the creep laws derived from a large number of creep tests and the fitting of experimental parameters [14]. By means of continuum damage mechanics (CDM) and the creep damage state variables, it is possible to numerically depict all three stages of creep to rupture, especially for the tertiary creep behaviour.

For this purpose, a number of creep damage models were proposed and studied. The comparative research was reported by Rouse [15], where the hyperbolic sine creep function

and the power law-based models, including Liu–Murakami and Kachanov-Robotnov, were compared to show the effectiveness and conservativeness of each model. For instance, the Kachanov-Robotnov creep model is more suitable than the Norton function when simulating the creep behaviour of Nickel-based alloy under a high-temperature environment [16]. The Liu–Murakami creep damage model is also able to calculate the creep crack growth life of 316H steel under the extended finite element method (XFEM) framework [17]. The damage evolution and stress redistribution of a 3D Bridgman notched specimen was clarified by the recently developed hyperbolic sine (Sinh) model, which gave out a better creep crack growth evaluation than other models [18].

Combined with commercial FEA software, Omega model-based engineering approach [19, 20] has been applied to high-temperature structure design and evaluation of pressure vessels, which may have a risk of creep-induced failure [21, 22]. Both API 579-1/ASME FFS-1 and ASME Boiler and Pressure Vessel Code Case 2605-3 include the Omega model-based method and provide detailed parameters and numerical procedures for the users [23, 24].

Instead of tracking the entire process of creep rupture failure, a different type of technique to deal with the creep rupture endurance was put forward by the high-temperature structure assessment procedure R5 [25], in which creep rupture data can be utilised directly to acquire rupture reference stress [26] by simplified elastic analysis and subsequently to quantify the creep significance by the creep usage factor. Following the methodology described, Chen [26, 27] proposed the extended Linear Matching Method (LMM) creep rupture procedure by combining both material's revised yield stress and the traditional shakedown analysis algorithm to provide an alternative to implementing non-linear creep rupture assessment and to minimize the conservativeness of simplified elastic analyses. It now has been integrated within the LMM framework to analyse the structures subjected to both monotonic and cyclic load conditions under elevated operating temperatures. Because of its concise linear iteration form, this algorithm can overcome the convergence difficulties faced by other non-linear creep simulation methods. The LMM framework is then further extended to address the creep-fatigue interaction problem by Chen and Groash, with the creep damage evaluated by the time fraction rule [28-33].

The aforementioned creep rupture assessment techniques, including ISS curve, Omega

creep damage model and LMM creep rupture analysis, have their characteristics, however, so far, there is no systematic research delivered before on these methods. It is necessary to recommend an in-depth examination to bridge the gap, providing a sufficient basis for selecting the appropriate creep rupture analysis method in engineering applications. Besides, inevitably, the material constitutive models and parameters to describe the creep behaviour are not consistent for different approaches due to unequal experimental calibrations, as a result, leading to unfair comparison. Therefore, this paper focuses on proposing a robust assessment technique to deal with creep rupture failure of high-temperature structures based on the unbiased comparative investigation of mainstream assessment techniques. And a deep and comprehensive understanding of the creep rupture failure mechanism is demonstrated with a complicated 3D benchmark. In addition, applicable creep rupture limit boundaries in terms of both monotonic and cyclic loading conditions are established not only for design purposes but also for evaluating the in-service high-temperature component against creep rupture failure, where the correlations between different mechanisms of shakedown, creep rupture and creep induced ratcheting are identified and clarified for the first time. Furthermore, aiming at confirming the effectiveness of such design curves, the creep rupture evaluation curves are validated in a new way through detailed step-by-step non-linear creep analyses, which makes such an engineering design tool reliable and robust when dealing with the assessment of creep rupture failure for the high-temperature components. All of these are the added values of our investigation for the industry.

This manuscript is organized as follows. In Section 2, there is a detailed review and comparison of the three methods from the theoretical view. Next, by applying the above three methods to a typical high-temperature structure, a hydrogenation reactor operating in the chemical industry is investigated numerically to calculate the creep rupture limit load in Sections 3 and 4. And, in Section 5, the creep rupture boundary acquired by the LMM creep rupture analysis is illustrated and an effective numerical verification strategy for the calculated creep rupture boundary above is proposed based on the step-by-step non-linear FEA. Finally, additional discussions of the case with cyclic loading conditions are elaborated in Section 6, and the main conclusions are listed briefly in the last section.

2. Methodologies of creep rupture limit analysis

2.1. The ISS curve-based creep rupture limit analysis

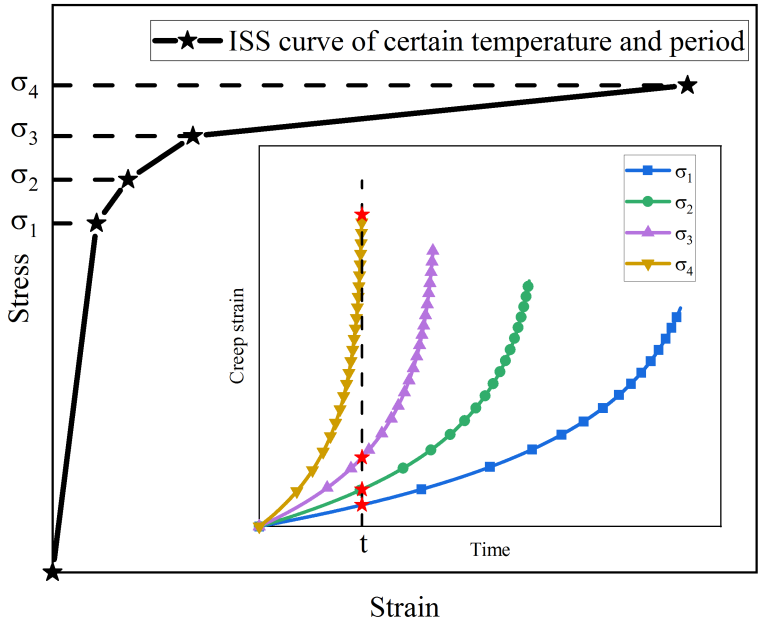

Fig. 1. Scheme of the isochronous stress-strain curve

Ideally, the material's ISS curve database comes from a large number of uniaxial creep tests, creating a series of long-term creep strain curves [34], during which the stress and temperature are kept constant for a certain creep period. As explained in Fig. 1, by extracting the stress and strain data at the same time point from the creep test curves above, an isochronous stress-strain curve similar to the material's elastoplastic constitutive relationship is constructed. Repeating the same steps and choosing the next time point, the ISS curves over a range of creep times and temperature magnitudes can be acquired sequentially. Through this transformation, the time-dependent creep process has been described in a time-independent form, reflecting the relationship between stress and total strain including elastic strain, creep strain, and plastic strain (defined in equation (1)) [11] under a fixed creep time.

$$\varepsilon_{total} = \varepsilon_{elastic} + \varepsilon_{plastic} + \varepsilon_{creep} \quad (1)$$

By substituting this ISS-based constitutive relationship for inelastic material's property,

the structural creep rupture limit is able to be calculated by the general elastoplastic FEA program. And the rupture failure state is determined at the physical instability point of the non-linear iterations, where the creep dwell period is considered implicitly in the material's constitutive relationship [13].

2.2. The strategy of the Omega creep damage model-based creep analysis

For the sake of evaluating the structure creep rupture life and remaining life numerically, Omega creep model was developed under the Material Properties Council (MPC) Omega Project, based on a large number of material tests and Kachanov's CDM concept [22]. Unlike the fundamental Norton's law that treats the secondary creep stage as the key factor, the Omega creep damage model focuses on the tertiary creep phase under the design stress level [20, 35]. By utilizing the exponential form of creep rate and its integral form below,

$$\dot{\varepsilon} = \dot{\varepsilon}_{oc} e^{(m+p+c)\varepsilon} \tag{2}$$

$$\frac{1}{\dot{\varepsilon}_{oc}(m+p+c)}\left(1 - e^{-(m+p+c)\varepsilon}\right) = t \tag{3}$$

the damage term Ω is defined by equation (4) physically and mathematically, including m, Norton's exponent to describe the rate increase because of the cross-section reduction effect; p, microstructural damage; and c, deficiencies in Norton's exponent and other microstructural factors related to the stress change [19], and calibrated by using the coefficient of the relative (logarithmic) change in strain rate during a creep test. Therefore, the time to creep rupture, t_r, is able to be estimated below,

$$\begin{gathered} \frac{1}{\dot{\varepsilon}_{oc}(m+p+c)} = t_r = \frac{1}{\dot{\varepsilon}_{oc}\Omega} \\ \Omega = m + p + c \end{gathered} \tag{4}$$

where the creep damage rate is also determined by $\dot{D}_c = \frac{1}{t_r} = \dot{\varepsilon}_{oc}\Omega$.

As shown in Fig. 2, there is a strong connection between the strain rate and the amount of damage, which can be defined by the equation (5):

$$\dot{\varepsilon} = \frac{\dot{\varepsilon}_{oc}}{1 - D_c} \tag{5}$$

When the creep damage accumulates to nearly 1.0, the creep rupture occurs with the creep

strain rate tending to infinity.

If needed, it can be integrated to clearly describe the relationship between the creep strain and time. Additionally, a more practical and effective way to utilise this method is to embed the creep damage model into the commercial FEA software such as ANSYS and ABAQUS, making this creep model function as a creep constitutive equation during the calculation of creep strain, damage and creep rupture time. Both ASME Code Case 2605-3 [24] and API 579-1/ASME FFS-1 [23] incorporate the Omega creep model into the assessment options of creep-induced failures, where the creep damage at the critical locations is restricted to below 1.0 in order to prevent the whole structure from the risk of creep rupture. The detailed algorithms and specified material property parameters for programming via the creep user subroutine are illustrated in Appendix A.

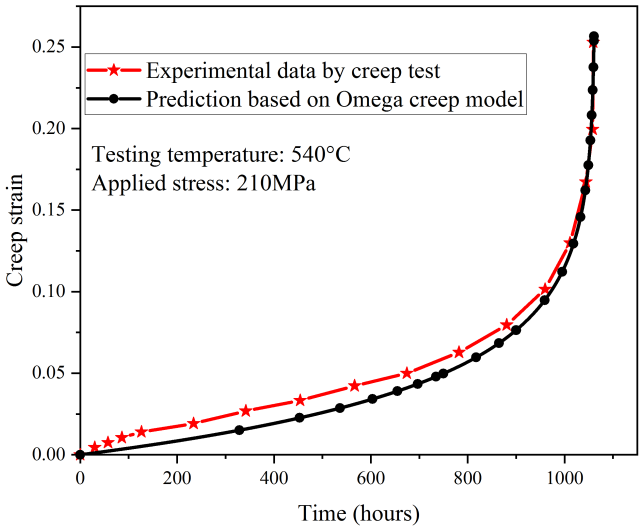

Fig. 2. Creep data of 2.25Cr-1Mo-V comparison between experiment and Omega model prediction

2.3. Numerical procedure of the LMM-based creep rupture analysis

The LMM creep rupture limit analysis is developed on the basis of an extended shakedown analysis procedure, depending on the concept of revised yield stress which is employed to substitute original yield stress by the minimum of the original yield stress and the creep rupture stress at a specified temperature when entering the creep temperature

range. The description of this program [26] is shown below.

It can be assumed that the material is isotropic and elastic-perfectly plastic (EPP), following the Mises yield condition. In the beginning, a linear solution $\lambda\hat{\sigma}_{ij}$ is determined in which λ is a parameter controlling the scaling of the load history applied. The process is based on incompressible and kinematic admissible strain rate history $\dot{\varepsilon}_{ij}^{c}$ which is associated with a compatible strain increment $\Delta\varepsilon_{ij}^{c}$ by integrating the following equation:

$$\int_0^{\Delta t} \dot{\varepsilon}_{ij}^{c}\, dt = \Delta\varepsilon_{ij}^{c} \tag{6}$$

where Δt is the period during the load cycle.

According to the shakedown upper boundary theory, a limit parameter λ_{UB_LIMIT} is calculated by

$$\lambda_{UB\_LIMIT} \int_V \int_0^{\Delta t} \left(\hat{\sigma}_{ij}\dot{\varepsilon}_{ij}^{c}\right) dtdV = \int_V \int_0^{\Delta t} \sigma_{ij}^{c}\dot{\varepsilon}_{ij}^{c}\, dtdV \tag{7}$$

When implementing a creep rupture limit analysis, σ_{ij}^{c} stands for either the stress near creep rupture or the stress at yield state with the strain rate history $\dot{\varepsilon}_{ij}^{c}$, and $\hat{\sigma}_{ij}$ is the linear elastic stress defined above, associated with the applied reference load history. Considering the associated flow rule, equation (7) can be transformed and the creep rupture limit multiplier is derived by the equation below:

$$\lambda_{UB\_LIMIT} = \frac{\int_V \int_0^{\Delta t} \sigma_y(t, t_r, T)\bar{\dot{\varepsilon}}\left(\dot{\varepsilon}_{ij}^{c}\right)dtdV}{\int_V \int_0^{\Delta t}\left(\hat{\sigma}_{ij}\cdot\dot{\varepsilon}_{ij}^{c}\right) dtdV} \tag{8}$$

where $\bar{\dot{\varepsilon}}$ is the effective strain and σ_y is the revised yield stress introduced before which is determined in equation (9) by the minimum of the creep rupture stress σ_r under certain creep dwelling time and the yield stress σ_s at the corresponding temperature.

$$\sigma_y(t, t_r, T) = min\{\sigma_r(t, t_r, T), \sigma_s(t, T)\} \tag{9}$$

This program consists of a series of iterations, starting with a history of plastic strain rate $\dot{\varepsilon}_{ij}^{i}$ and leading to a new strain history in the next iteration $\dot{\varepsilon}_{ij}^{new'}$,

$$\dot{\varepsilon}_{ij}^{new'} = \frac{1}{\mu}\left(\lambda_{UB\_LIMIT}^{i}\hat{\sigma}_{ij} + \bar{\rho}_{ij}^{new}\right)' \tag{10}$$

$$\dot{\varepsilon}_{kk}^{new} = 0 \tag{11}$$

where the symbol $'$ represents the deviatoric component, $\bar{\rho}_{ij}^{new}$ is the constant residual

stress field, and $\dot{\varepsilon}_{kk}^{new}$ is the hydrostatic component of the new strain rate history in the next cycle. The condition below provides the matching relationship to strictly guarantee that both EPP and linear material properties give the same response due to $\dot{\varepsilon}_{ij}^{i}$ defined at the beginning of this iterative step.

$$\mu = \frac{\sigma_y(t, t_r, T)}{\bar{\dot{\varepsilon}}^i} \tag{12}$$

The integral forms of these equations are as follows,

$$\Delta\varepsilon_{ij}^{new\prime} = \frac{1}{\bar{\mu}}\left(\bar{\rho}'^{f}_{ij} + \sigma_{ij}'^{in}\right) \tag{13}$$

$$\sigma_{ij}'^{in} = \bar{\mu}\left\{\int_0^{\Delta t} \frac{1}{\mu(t)} \lambda_{UB}^{i} \hat{\sigma}_{ij}'(t)dt\right\} \tag{14}$$

$$\frac{1}{\bar{\mu}} = \int_0^{\Delta t} \frac{1}{\mu(t)} dt \tag{15}$$

which gives the amount of these variables after an iteration. Next, as illustrated in Fig. 3, the modulus is modified according to the magnitude of the calculated strain in order to make the stress equal to the revised yield stress [36].

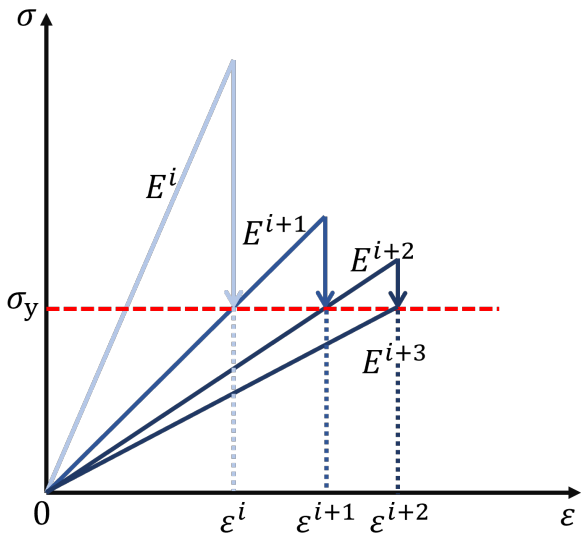

Fig. 3. Iteration process of the LMM-based creep rupture analysis

Repeating the steps above produces a set of monotonically decreasing upper bound multipliers, given by the following formula (16) until the iteration converges to a stable value.

$$\lambda_{UB\_LIMIT}^{new} \leq \lambda_{UB\_LIMIT}^{i} \tag{16}$$

It is worth noting that the LMM creep rupture analysis generates both the upper bound multiplier and the lower bound multiplier for the creep rupture limit simultaneously. However, the upper bound solution based on the energy criterion gives out more accurate results than the lower bound solution, as the lower bound solution is very model-sensitive and depends on the stress solutions at the most critical location. Therefore, the LMM upper bound creep rupture limit results are utilised for all the discussions in this study.

According to a convex yield condition, several straight-line paths and vertices in the load space are adopted for engineering problems to predefine the load history. As these vertices correspond to the appearance of plastic strain, the sum of plastic strain increments at each vertex results in the strain increment over a certain cycle. In particular, if the load path is prescribed by only one condition point in the load space, this iteration form degenerates to a creep rupture limit analysis under the monotonic load condition, which paves the way for solving the creep rupture limit problem by the extended LMM algorithm.

3. Problem description of creep rupture assessment for hydrogenation reactor

In this section, a typical high-temperature structure, the hydrogenation reactor component, is chosen as the benchmark to investigate the aforementioned creep rupture limit analyses numerically. As a large-scale pressure vessel, the hydrogenation reactor is the core operating unit of the petroleum refining and coal chemical industry, running under elevated temperature and complex mechanical load conditions. Hence, when designing and assessing this equipment, creep rupture is the most crucial failure mode among several potential failure behaviours.

3.1. FEA model description

Due to the symmetry of this structure, a quarter model of the component, a hydrogenation reactor with a normal nozzle, is created in ABAQUS CAE, with its inner radius of the main vessel 1500 mm and thickness of 130 mm. This structure is meshed by the 20-node quadratic brick element C3D20 and refined around the welding transition zone

between the main vessel and nozzle (see Fig. 4 and Fig. 5) to capture the high-stress gradient effect. As to the nozzle part, its inner radius is 108mm and its thickness is 122 mm. Along the thickness direction, the pressure vessel is discretised into 9 elements, with the adopted minimum element size of 4.2 mm, which is sensitive enough to meet the requirement for the mesh convergence check. It is worth noting that the creep rupture is a global failure mode of the whole structure, and hence the creep rupture limit is not sensitive to the accuracy of the local stress and strain solutions. That means the linear element is also acceptable if the computational resource is limited.

This hydrogenation reactor is made of 2.25Cr-1Mo-V steel because of its high strength, extraordinary anti-hydrogen embrittlement property, and creep rupture resistance [35]. The basic material's properties including Young's modulus E, yield stress σ_s, and coefficient of thermal expansion α are presented in Table 1 and the Poisson's ratio ν at all design temperatures is set to 0.3.

Table 1

Material properties of 2.25Cr-1Mo-V steel for a given temperature from Ref. [37]

Temperature/°C	E/GPa	σ_s/MPa	$\alpha/\times 10^{-6}°C^{-1}$
400	184	353	15.9
425	/	346	16.1
450	180	339	16.4
475	/	332	16.5
500	175	324	16.7

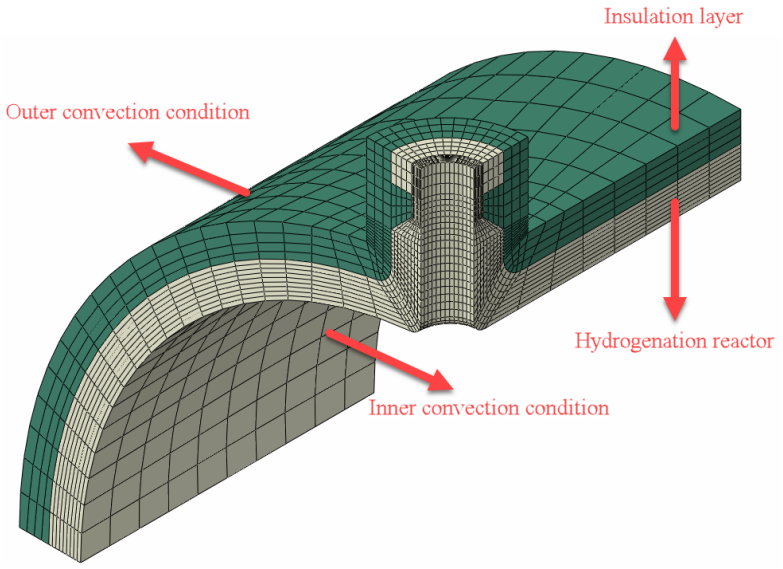

Fig. 4. Finite element model and Convection conditions for thermal analysis (insulation layer and steel pressure vessel)

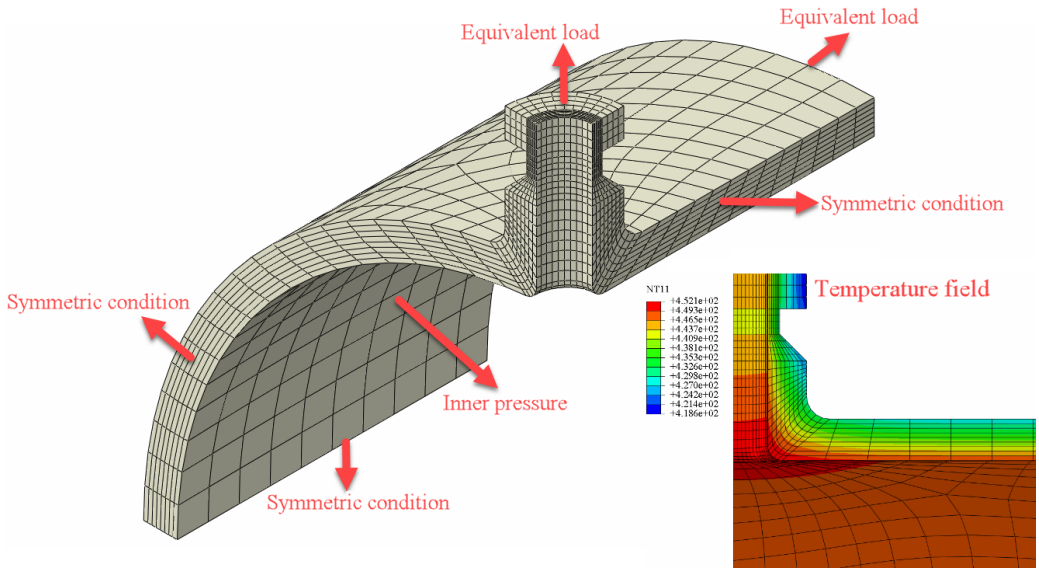

Fig. 5. Finite element model and boundary conditions for creep rupture analysis (only pressure vessel)

Indeed the adoption of the same material properties is the key prerequisite to guarantee the effectiveness of this investigation, however, the direct use of real creep properties in different forms inevitably makes the comparative study biased since different methods rely on unequal material parameters calibrations to describe creep behaviour and these material parameters in different forms may not be consistent. To avoid such an issue, an alternative

is adopted that the same creep deformation curves acquired from the virtual creep test, where the Omega creep model plays the role of the constitutive relationship to generate the ISS curve and related creep rupture stress for the other two methods respectively, hence, making later investigation on the unified material base.

Therefore, in this study, the ISS curves and the creep rupture stresses for given service lives and temperatures are derived by a series of virtual creep experiments numerically in which the Omega creep constitutive equation (5) is integrated via the ABAQUS user subroutine, acting as the creep strain rate function in the FEA test with a single element. In this way, different methods are placed under the same material data source, and the study fully reflects the inherent differences between these methods. The virtual experimentally generated creep test curves for 2.25Cr-1Mo-V steel are shown in Fig. 6, and Fig. 7 displays the related ISS curves, with the typical operating temperatures (425°C and 450°C) and working period (250,000 hours) of the hydrogenation reactor selected. Fig. 8 provides the revised yield stress data used by the LMM creep rupture analysis to consider the creep rupture failure, which is determined according to the minimum of the normal material's yield stress and creep rupture stress under specified temperature level and service life. The calculation paths of the three strategies are summarised in the flowchart in Fig. 9, where the input requirements and result forms of each are exhibited.

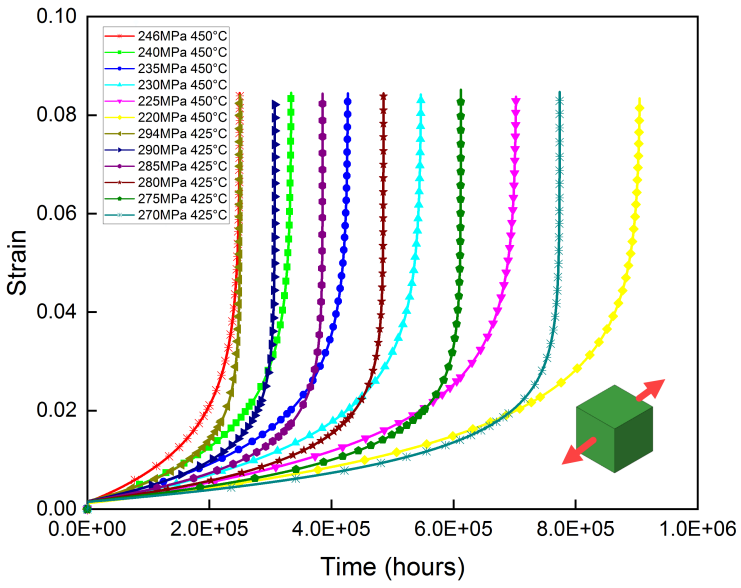

Fig. 6. Virtual creep experiments curves for 2.25Cr-1Mo-V under different conditions derived from the Omega creep model

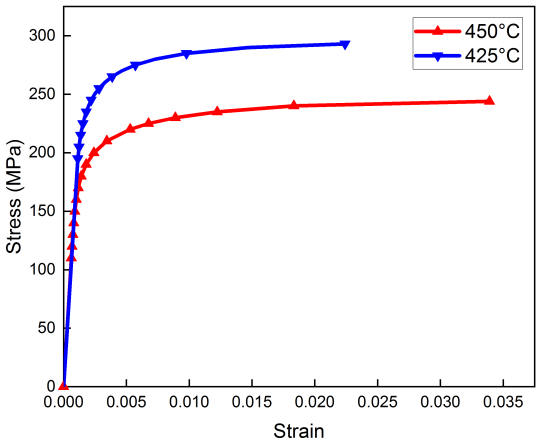

Fig. 7. ISS curves of 2.25Cr-1Mo-V steel for 2.5 ×105 hours

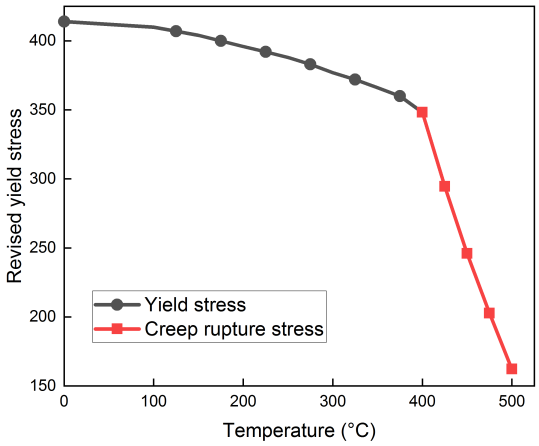

Fig. 8. Revised yield stress of 2.25Cr-1Mo-V steel for 2.5 ×105 hours

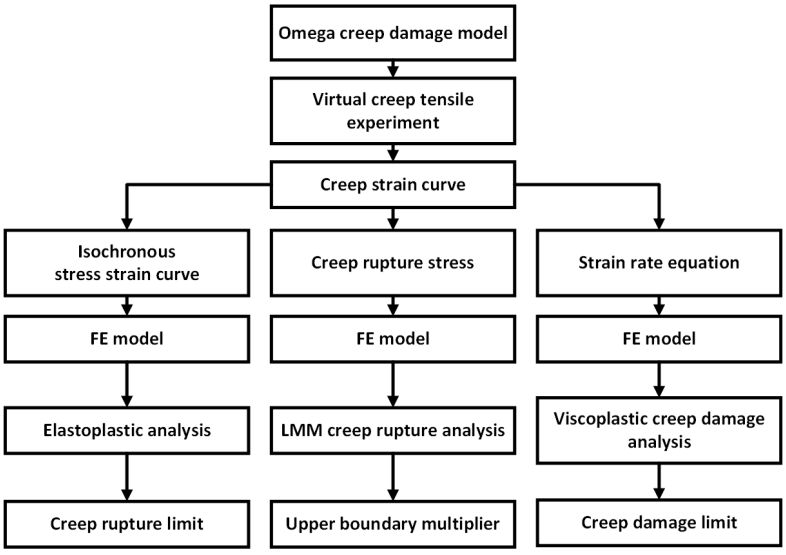

Fig. 9. Flowchart of three creep rupture limit analysis strategies

3.2. Boundary conditions

Aiming at determining the temperature distribution among the structure, a hydrogenation reactor model covered with an insulation layer is created for the thermal analysis, where two convection conditions (shown in Fig. 4 and Table 2) are applied on both inner and outer surfaces, respectively, providing the temperature field for subsequent creep rupture limit analyses. For creep rupture limit analysis, in addition to the temperature field (displayed in Fig. 5) imported from the above thermal analysis, the inner surface of

the vessel is subjected to a high-pressure load, with the related equivalent loads at the end of the nozzle and right side of the main vessel added. The symmetric boundary conditions are also applied to the other three end surfaces, which are illustrated in Fig. 5.

Table 2
Convection condition parameters for thermal analysis

Convection condition	Inner surface	Outer surface
Film coefficient/W/mm^2·°C	1.2×10^{-3}	1.2×10^{-5}
Temperature/°C	454	-20

For the ISS-based method, the applied pressure should be large enough to reach the rupture limit load during the non-linear FEA. As to the Omega model-based creep approach, a series of trial and error searches are performed continually to seek the final acceptable load condition which leads to the threshold of creep damage. By contrast, in LMM creep rupture analysis, only a reference load is needed, which is usually set to one unit (1 MPa in this case).

4. Comparative investigation of creep rupture analyses

4.1. Discussion on calculation processes and results

From the results displayed in Fig. 10, different result layouts are plotted to describe the creep rupture failure mechanism that after running for 250,000 hours, and the maximum creep strain, up to 0.0208, occurs at the inner corner of the nozzle connected to the main vessel cylinder. The creep strain produced around the inner corner gradually decays to the minimum level along the axial direction of both the nozzle and vessel cylinder, respectively, while the rest of the material remains undamaged.

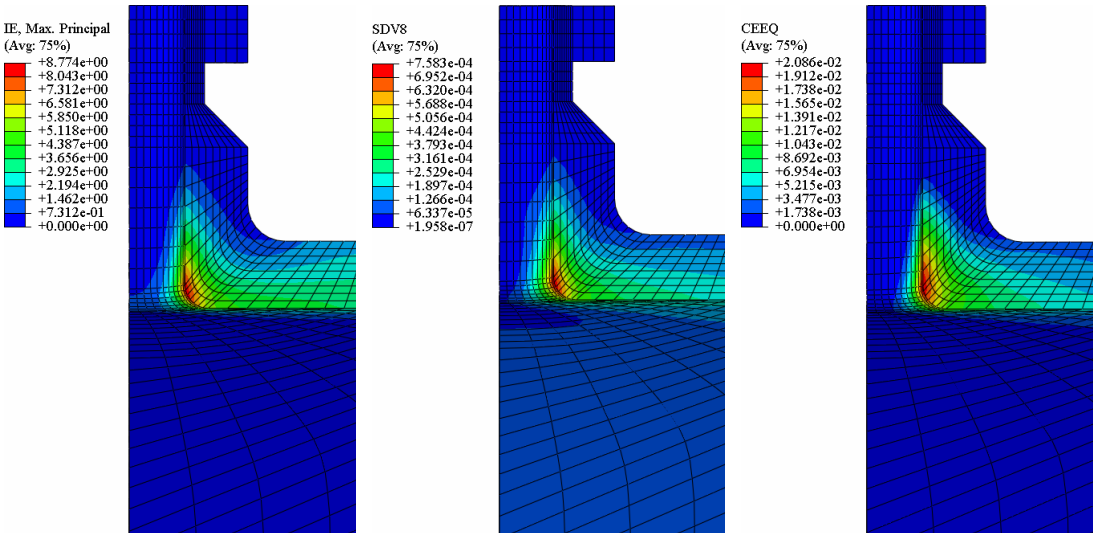

(a) (b) (c)

Fig. 10. Failure mechanism by creep rupture analyses after 250,000 hours: (a) Inelastic strain by ISS curve-based analysis; (b) Effective strain increment by LMM creep rupture analysis; (c) Creep strain by Omega model-based analysis

Based on the elastoplastic analysis, the ISS curve-based approach considers the inelastic strain (see Fig. 10a) as the creep strain. Alternatively, the distribution of inelastic strain increment (see Fig. 10b) is employed by the LMM creep rupture analysis to demonstrate the failure mode. While, only by Omega model-based creep simulation, the creep strain (Fig. 10c) can be acquired by embedding a creep user subroutine into the FEA.

Additionally, the interpretations of the stress result further explain their features. Relying on the stress level to define the material's failure state, both the ISS curve-based analysis and LMM creep rupture analysis present a final stress state after 250,000 hours described in Fig. 11 that is similar to the plastic flow state due to yielding. The stress values of the keypoint defined by the maximum creep strain (in Fig. 10) correspond to either maximum isochronous stress or revised creep rupture stress under specified temperature and dwell time.

On the other hand, as a time history analysis, the viscoplastic FEA with the Omega creep model generates detailed information on every step during the creep evolution, providing sufficient insight into stress relaxation and creep damage accumulation. After a short loading stage, the high-stress region induced by non-primary load begins to relax to a stable level. Simultaneously, in other regions, the relatively low stress increases gradually,

leading to a stress redistribution which makes the local stress field at the transition region, connecting the main vessel and nozzle, tend to be more uniform, as shown in Fig. 12. This stress redistribution results from the attribution of the self-equilibrating residual stress field that ensures an equilibrium with the external load. As the creep damage is controlled by the combination of stress level, working temperature and creep dwell, the critical location of creep damage may shift with the stress redistribution when the dwell time progresses, which is different from the case of fatigue-induced failure where the critical location normally keeps unchanged. During the tertiary creep stage, with the creep damage continuously cumulating (see Fig. 13), the creep strain rate starts to accelerate, leading to the subsequent creep crack initiation and propagation.

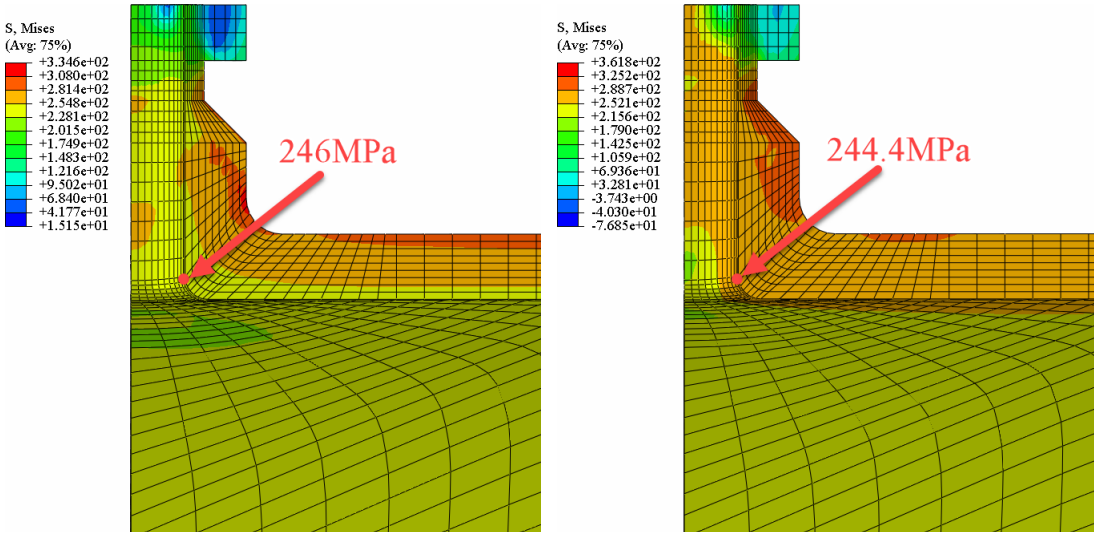

Fig. 11. Stress distribution after 250,000 hours operation: (a) By ISS curve-based analysis; (b) By LMM creep rupture analysis

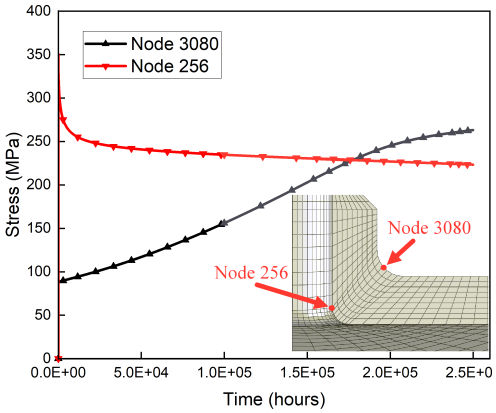

Fig. 12. Stress redistribution process by Omega model-based analysis

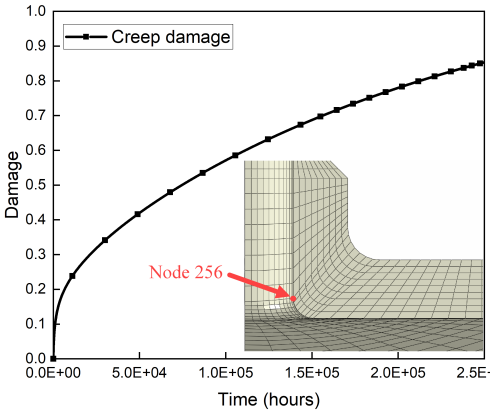

Fig. 13. Creep damage accumulation by Omega model-based analysis

Table 3 compares the results of the creep rupture limit of the reactor under the predefined temperature field in Fig. 5 for 250,000 hours of dwell period. It can be seen that the creep rupture limit calculated by the Omega model-based analysis is quite lower (21.30 MPa, about 12% to 14% less than the other two methods) than the others which produce two close limit values, 24.95 MPa and 24.19 MPa, respectively. Essentially, the failure criterion of the Omega model-based creep assessment is dependent on the creep damage state variable (SDV 2 in Fig. 14) of one significant node that reaches nearly 1.0, which makes equation (5) tend to diverge numerically. However, at the same time, the local materials surrounding the first failed node have not cumulated enough creep damage at all, which is observed from the creep damage distribution (around the inner corner of the nozzle) after 250,000 hours in Fig. 14. Therefore, the Omega model-based creep assessment produces a conservative result if the acceptable design load is determined based on the damage of a single node since this structure is able to withstand an additional load until the final rupture.

Exceptionally, if the interest is aimed at calculating the ultimate limit, the ABAQUS user subroutine USDFLD should be additionally employed to adjust Young's modulus at each damaged integration point along the specified path, so that the damaged elements are able to simulate the subsequent crack propagation from the initial crack tip. Moreover, in order to capture the crack propagation features, the element number along the potential fracture path should be refined with a large mesh density to alleviate the trouble of

convergence difficulties during the sharp change in element stiffness. And, unavoidably, this poses an inevitable challenge for the computing resources, which, consequently, limits the application of this method only to the specimen structures stage at present instead of engineering structures.

Concerning the ISS curve-based approach and the LMM creep rupture analysis, the final creep rupture of the structure takes place once the material in a considerable region (see Fig. 11) meets the creep damage criterion, either the maximum isochronous stress (for the ISS curve-based method) or the revised creep rupture stress (for LMM creep rupture analysis). The creep rupture mechanism calculated by these two methods is more consistent with the actual fracture failure, where the creep rupture region in the structure consists of a large number of fully creep damaged elements.

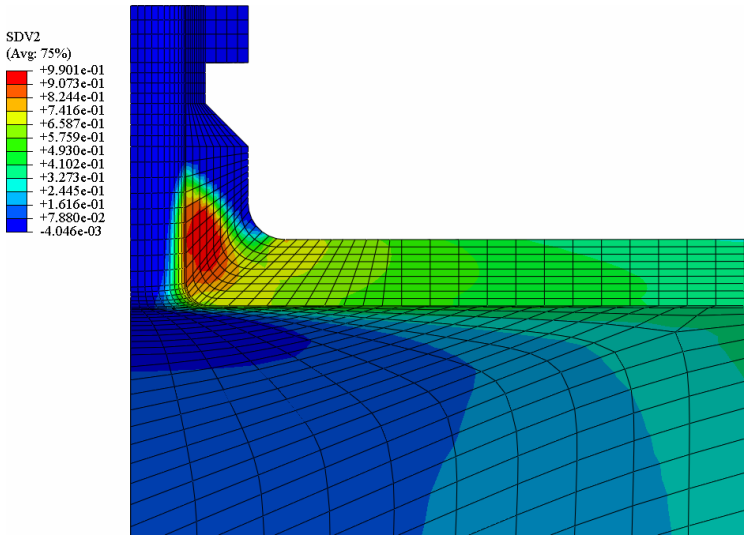

Fig. 14. Creep damage distribution after 250,000 hours by Omega model-based analysis

Table 3
Results of creep rupture limit load by three methods

Creep rupture analysis type	Creep rupture limit/MPa	Difference of rupture limit/%	Iterations	Difference of iterations/%
LMM-based analysis	24.19	/	60	/
ISS curve-based analysis	24.95	3.1418	116	93
Omega model-based analysis	21.30	-11.9471	7218	11930

4.2. Discussion on computational efficiency

Besides the conservativeness, computational efficiency is another obvious discrepancy between these methods that should be discussed. In Table 3, the number of iterations is considered as the total number of numerical iterations consumed in ABAQUS during the whole process of running FEA programs. And the computational performances of different creep rupture analysis approaches are compared in Fig. 15. There is no doubt that the Omega model-based creep method consumes the most iterations, 7218 times (in orange colour), among all three strategies, which is 120 times that of the LMM-based creep rupture analysis (in purple colour) and 62 times that of the ISS curve-based analysis (in green colour). Although this time history analysis has the capacity to simulate the exact evolution of each important result such as creep strain, creep damage and stress relaxation and redistribution over the creep dwelling period (see Figs. 12 and Fig. 13), this strategy appears redundant if the core problem of evaluation is to obtain the creep rupture limit as a design parameter for structures. Besides, when reaching the end of the tertiary creep stage depicted by CDM-based creep damage models, the creep strain rate in equation (5) and creep strain soar rapidly even if an extremely tiny time increment is applied, which results

in the difficulty in the convergence of the numerical calculation. Not to mention that subsequent fracture mechanics simulation may be required to solve the ultimate rupture load. Consequently, to prevent the FEA program from numerically diverging, the time increments have to be set as a series of tiny values, which causes a great consumption of computing resources. Facing a similar obstacle, the ISS curve-based inelastic approach employed the Newton-Raphson iteration scheme to solve non-linear problems [38] so that when approaching the physical instability or encountering convergence difficulties, predicting the creep limit accurately needs a large number of equilibrium iterations (116 times in this case) in spite of being lower than the cost of Omega model-based analysis.

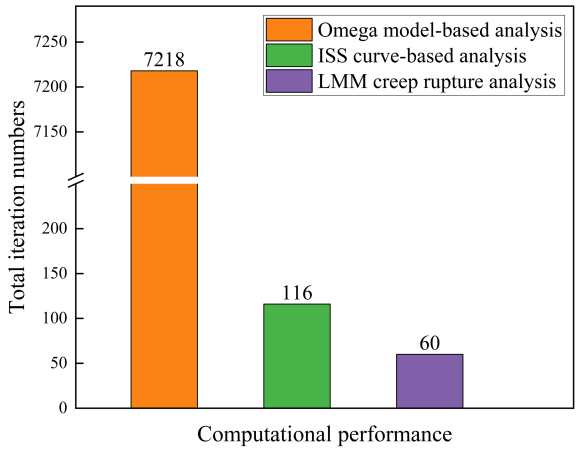

Fig. 15. Comparison of the computational efficiency of different creep rupture analyses

On the contrary, because of utilizing a more efficient iteration form, the LMM-based creep rupture analysis method performs a series of linear solutions (equations from (6) to (16)) to match the material's non-linear behaviour based on the extended upper bound shakedown theory, which adopts a significantly lower number of iterations (consumed 60 times in this case) than the other two methods.

To summarize, although the Omega creep damage model is capable of providing detailed creep strain and creep damage information during the creep development process, it consumes too much computational resource during simulation. In addition, according to the API 579-1/ASME FFS-1[23] and ASME Boiler and Pressure Vessel Code Case 2605-3 [24], there are 10 related material parameters to depict the creep behaviour of the specified material. Besides, the failure threshold is only defined by the creep damage of

one critical location, which finally produces acceptable but over-conservative load conditions. The ISS curve-based method needs the isochronous stress-strain curves data under a certain range of dwell periods and operating temperatures, which are derived from either long-term creep tests or the mathematical extrapolation [39] of short-time creep experiment data. However, when the Newton-Raphson iteration needs very tiny increments, its calculation process still faces the problem of difficulty in convergence. By contrast, with only one key parameter included, the revised yield stress, the LMM-based creep rupture analysis shows a more reasonable creep rupture limit for engineering design and evaluation than others. Moreover, by running a series of more robust and efficient linear algorithms, the LMM-based method costs the least amount of computing resources.

5. Creep rupture limit boundary of hydrogenation reactor

5.1. Creep effect on limit boundary

Apart from calculating the creep rupture limit under specified load conditions, a more useful capability of the LMM creep rupture analysis is to construct the limit boundary including the mechanical load and thermal load. By selecting a series of load points sequentially in the load space (usually according to the ratios of different load combinations), the hydrogenation reactor's creep rupture limit boundary for 250,000 hours dwelling period (shown in solid red line) and the normal limit load boundaries (shown in black dash line) are constructed in Fig. 16. Here, the coordinates of vertical and horizontal axes are normalised by the initial temperature condition $T_0 = 454\,℃$ and the limit pressure without any creep effect $P_0 = 38.52MPa$, respectively.

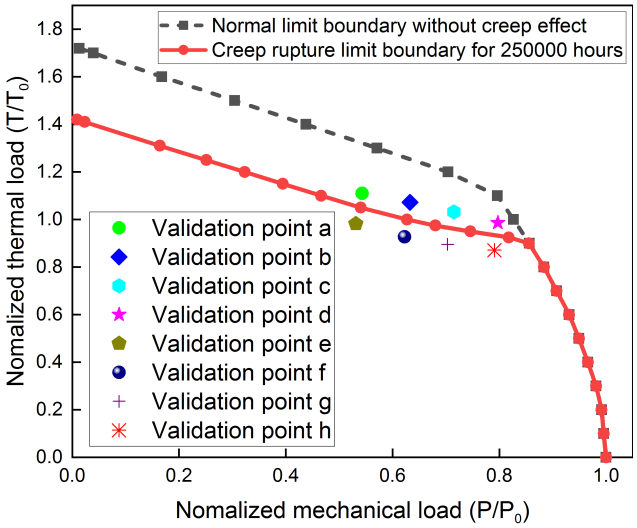

Fig. 16. Temperature-dependent normal limit load and creep rupture limit boundaries by LMM analysis

At the bifurcation location of two curves, a definite turning point divides the structural response into the high-temperature dominated zone and mechanical load dominated zone. Above this turning point, the failure mode is mainly influenced by the creep rupture under the high-temperature condition, and the acceptable mechanical load decreases gradually with the increasing thermal condition. In contrast, when below this turning point, the revised yield stress in the LMM creep rupture analysis algorithm is controlled by the material's yield stress. The creep-induced weakening effect reduces or disappears, and the excessive plastic deformation-induced failure mode takes over the dominant factor, leading to plastic instability or plastic collapse as the monotonic mechanical load approaches the limit on the boundaries.

Compared to the limit load boundary without the creep effect, the acceptable load domain shrinks inward dramatically under the elevated temperature, which means that the creep effect on the limit boundary appears only at the high-temperature zone above the turning point. This is because, under elevated temperature conditions, the revised yield stress is determined by the creep rupture stress which is much lower than the normal yield stress.

It is worth noting that normally, the effect of high-temperature conditions on structural failure is manifested in two forms: thermal stress and weakening of key material strength

parameters. In this case, the thermal stress is secondary stress, which is self-balancing stress, and, hence, makes no contribution to the limit load. However, the weakening of material strength parameters under high-temperature conditions, including yield stress and creep rupture stress, is the significant factor affecting the limit load. Consequently, this also results in the shape of the two limit curves in high-temperature regions. Even under extremely small mechanical loads, the limit curves are only close to the y-axis and have no intersection with the y-axis.

5.2. New verification strategy of creep rupture boundary

In order to further verify the effectiveness of the creep rupture boundary curve by LMM creep rupture analysis, validation work has been provided by Ref. [27], where the creep rupture stress functions as the standard yield stress during the step-by-step inelastic FEA program. However, this method is only able to test the effectiveness of the extended LMM shakedown procedure with the revised yield stress employed, and it is not capable of directly verifying the creep rupture limit associated with a predefined dwell time.

In this section, a new verification strategy for the creep rupture boundary is proposed to consider creep damage development. Firstly, the checkpoints are arranged according to the creep rupture boundary calculated by the LMM creep rupture analysis, where checkpoint A is just inside the creep rupture boundary, and checkpoint B is selected slightly above the boundary. Then, the conditions of checkpoints are applied to the FEA model to perform the detailed creep analysis with the Omega creep model. If the calculated creep rupture boundary is accurate, checkpoint A should produce a creep failure time larger than the predefined creep rupture time, whereas the creep failure time of checkpoint B should be less than the predefined time. The flowchart below illustrates this verification strategy for creep rupture boundary, as shown in Fig. 17.

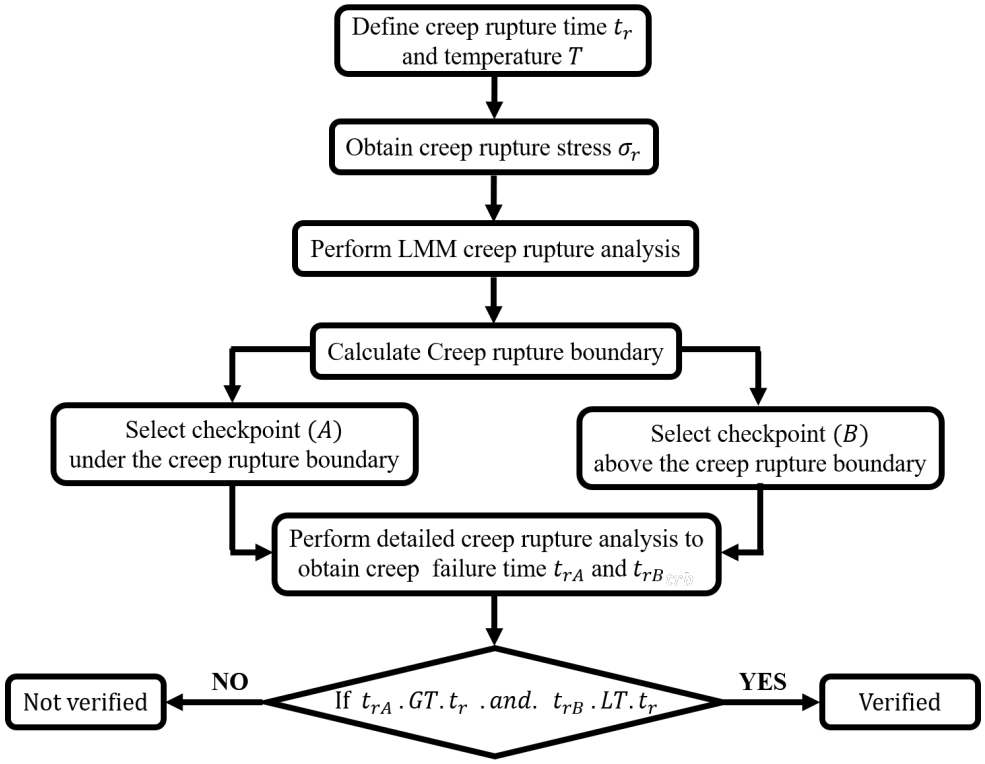

Fig. 17. Flowchart of verification strategy for creep rupture boundary

Four pairs of checkpoints are chosen in the load space at the following location: (a) (0.54292, 1.110), (b) (0.63278, 1.072), (c) (0.71504, 1.032), (d) (0.7973, 0.986), (e) (0.53128, 0.982), (f) (0.62265, 0.9275), (g) (0.70314, 0.895), (h) (0.79097, 0.871) in **Error! Reference source not found.**. All the condition points are determined according to the most commonly used operating temperature conditions of hydrogenation reactor, ranging from 395 ℃ to 495 ℃ [40], among which checkpoints (a), (b), (c) and (d) are just above the creep rupture limit boundary, slightly outside the acceptable domain. While, accordingly, checkpoints (e), (f), (g) and (h) are selected inside the safe region near the boundary. Here, the detailed creep analysis is adopted to verify the accuracy of the creep rupture boundary under all the load conditions.

The verifications are listed in Table 4, and it can be seen that as the creep damage variable (output by ABAQUS SDV value) accumulates to the limit (the threshold of creep damage is equal to 1.0), all load points outside the creep rupture limit boundary (including (a), (b), (c) and (d)) exhibit the creep rupture failure. The creep rupture time under these

conditions is significantly less than the period (250,000 hours) which is prescribed by the corresponding creep rupture boundary.

Instead, when inside the acceptable regions, the creep behaviour of 250,000 hours of dwelling periods under each load condition satisfies the requirement of creep limit, and, at the same time, the creep damage variables at the predefined keypoint are lower than the threshold value (creep damage equals to 1.0), with their values 0.9827, 0.9842, 0.9881 and 0.9811, respectively (see detailed creep FEA results from Fig. 18 (e) to (h)). In other words, if the structure is subject to the load conditions determined by checkpoints (e), (f), (g) or (h), the maximum acceptable creep dwelling periods can be extended to a longer time, 267,012 hours, 272,531 hours, 262,311 hours and 268,630 hours, respectively. It is worth noting that all the checkpoints selected here are aimed at reflecting the response of the structure and accuracy of the boundary at the elevated working temperature, where the creep effect plays a more dominant role, hence avoiding the influence of plastic yield due to high mechanical load as much as possible.

Table 4

Verification of the creep rupture boundary constructed by LMM creep rupture analysis

Checkpoint		Location	Maximum creep dwelling time/hours
Outside	(a)	(0.54292, 1.110)	Up to 232675
	(b)	(0.63278, 1.072)	Up to 238164
	(c)	(0.71504, 1.032)	Up to 230922
	(d)	(0.79730, 0.986)	Up to 231981
Inside	(e)	(0.53128, 0.982)	Up to 267012
	(f)	(0.62265, 0.9275)	Up to 272531
	(g)	(0.70314, 0.895)	Up to 262311
	(h)	(0.79097, 0.871)	Up to 268630

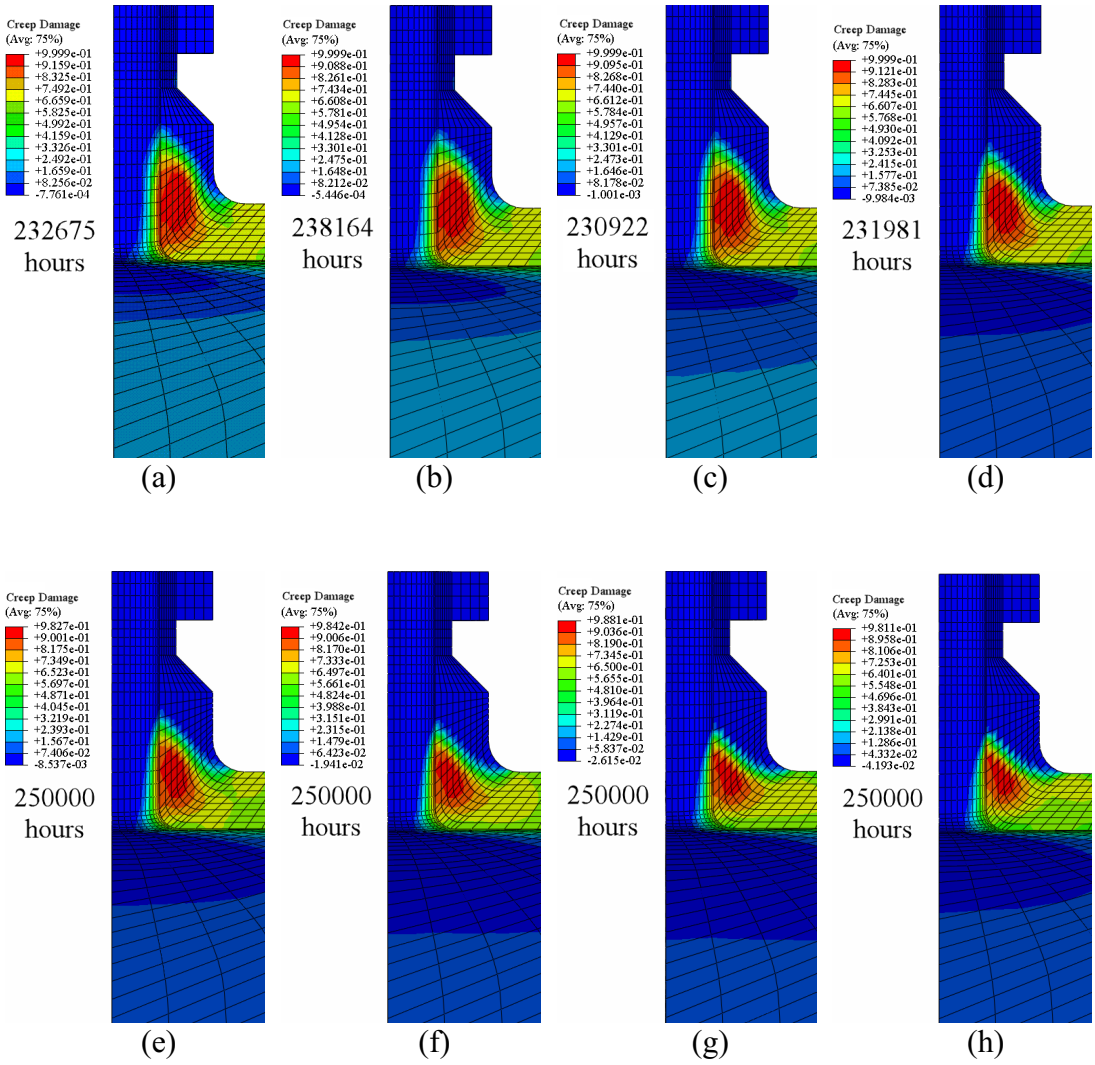

Fig. 18. Creep damage for verification cases: (a) creep damage under condition a; (b) creep damage under condition b; (c) creep damage under condition c; (d) creep damage under condition d; (e) creep damage under condition e; (f) creep damage under condition f; (g) creep damage under condition g; (h) creep damage under condition f; (g) creep damage under condition h

6. Further discussions of creep rupture assessment with cyclic load conditions

When extending the monotonic load condition to the cyclic one under a high-temperature environment, creep-fatigue interaction is viewed as a complicated failure behaviour by Refs. [41, 42]. Due to the severe combinations of mechanical and thermal loads, the cyclically enhanced creep and creep-enhanced plasticity interact simultaneously, leading to creep-fatigue damage accumulation. However, the creep rupture is the first

considered failure mode that should be avoided for equipment under high-temperature conditions.

Adopting the cyclic load path prescribed in Fig. 19, a cyclic creep rupture assessment is also able to be performed by the LMM-based creep rupture analysis where both mechanical load and thermal load conditions are assumed to be cyclic. Following the same strategy adopted when dealing with the monotonic loads, in Fig. 19, the black line represents the normal elastic shakedown boundary, while the cyclic creep limit boundary for 250,000 hours is presented by the red line, with an obvious inward contraction compared with the shakedown boundary.

Here, three typical failure mechanisms are distinguished by the different zones in terms of the limit boundaries of the cyclic load. The first one is when located outside the shakedown boundary, the hydrogenation reactor structure experiences the plastic ratcheting behaviour for the sake of excessive cyclic plastic deformation, with the plastic strain accumulating after every operation period, which has been verified by Chen [43, 44].

Secondly, considering the load condition under the cyclic creep limit boundary, since the stress relaxation has fully developed to a steady state, all subsequent loading and unloading keep repeating elastically in every cycle, without any plastic behaviour. As a result, this structure shows a general shakedown phenomenon, and finally, the creep rupture failure occurs at the limit time specified by the corresponding boundary. The load condition point 1 is defined to exhibit this cyclic response by a step-by-step creep analysis, and the cyclic stress-strain curve in Fig. 20 verifies this mechanism. Although the plastic behaviour occurs during the first cycle, this cyclic load combination dominated by the primary load cannot generate continuous stress relaxation in the subsequent cycles, which is identical to the monotonic load case. That means under load condition 1 the cyclic loading behaviour makes no contribution to the final creep rupture failure.

The last failure mode is when the load condition point moves into the intermediate region between the shakedown boundary and the cyclic creep limit boundary. Here, the response of this load condition (that should have caused an elastic shakedown state similar to behaviour under condition 1 if there is no creep effect involved) changes to the creep effect induced ratcheting or creep ratcheting [45, 46]. By validation result under load condition 2 (illustrated in Fig. 21), it can be observed that the increase of creep-induced

inelastic strain makes the reverse plastic yield and elastoplastic unloading always exists after each creep dwell step. And this load condition pushes the unclosed stress-strain hysteresis loops forward, keeping accumulating the cyclic inelastic strain cycle-by-cycle. In this response, the significant creep strain increment produced by the creep dwell period cannot be fully compensated by the reverse plastic strain during the unloading stage, which results in the open hysteresis loop. Compared with the second failure mode, the cyclic inelastic behaviour elevates the stress level at the start of each creep dwell period, making it much higher than the previous end of dwell stress, thereby strengthening the creep damage cyclically.

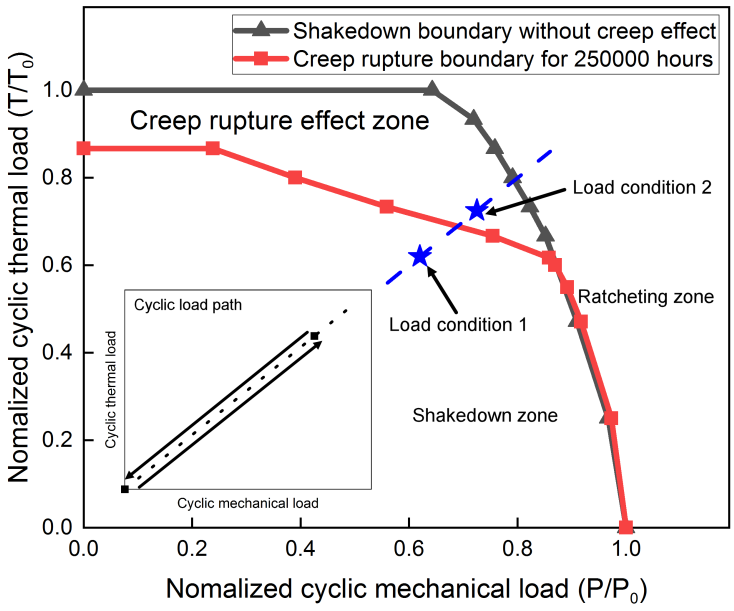

Fig. 19. Limit condition boundaries for cyclic load condition by LMM extended shakedown analysis

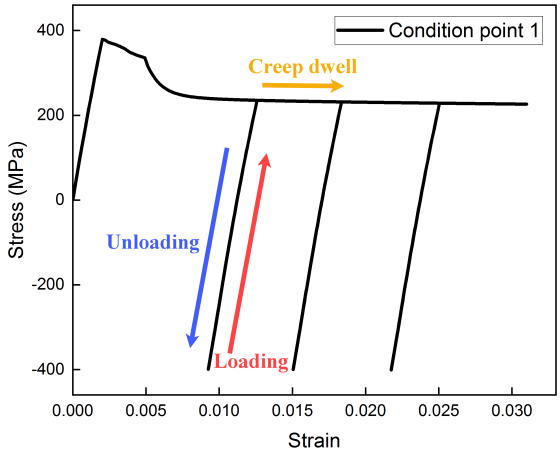

Fig. 20. General cyclic behaviour for load condition 1

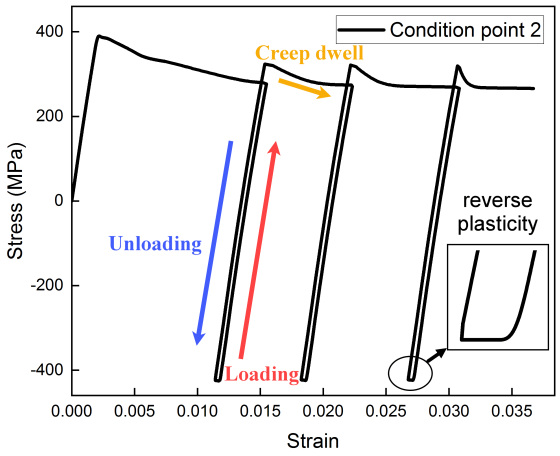

Fig. 21. General cyclic behaviour for load condition 2 (creep-induced ratcheting)

7. Conclusions

This paper presents a detailed comparative investigation of creep rupture limit analysis techniques in engineering assessment based on the unified material data, including the ISS curves, the Omega creep damage model and the LMM creep rupture analysis. Three approaches are implemented by using ABAQUS with the user subroutines to assess the high-temperature pressure vessel component with creep rupture risk, providing a deep understanding of creep rupture failure mechanisms and comprehensive insight into creep rupture evaluation techniques from different views. The main conclusions of this study are as follows:

1. Although according to the ASME Boiler and Pressure Vessel Code Case 2605-3, the Omega creep damage model-based analysis can simulate the entire history of the creep damage evolution and predict the dangerous location, it seems time-consuming and conservative to determine creep rupture limit, since the initial damaged node is not suitable to indicate the creep rupture failure of the whole structure.

2. The proposed LMM creep rupture analysis is a concise and robust tool to address the creep rupture limit problem, providing a reasonable creep limit and clear creep rupture failure mechanism, which achieves a good balance between accuracy and efficiency.

3. In the engineering application, a creep rupture limit boundary for 250,000 hours dwelling period is given out by the LMM numerical scheme, where the acceptable domain

is divided into two regions in terms of different failure mechanisms.

4. A numerical strategy is also proposed to verify the creep rupture boundary by the LMM creep rupture analysis, showing that this boundary can identify the acceptable domain in the load space composed of mechanical and thermal loads, which could be employed as a design and assessment tool for the high-temperature structures.

5. When evaluating more complicated cyclic load conditions, the LMM-based creep analysis also has the capability to scheme different failure regions, including general shakedown, plastic ratcheting and creep-induced ratcheting.

Acknowledgements

The authors gratefully acknowledge the support from the Royal Society, the National Natural Science Foundation of China (51828501, 52150710540 and 51911530201), the East China University of Science and Technology and the University of Strathclyde during the course of this work.

References

[1] Horseman G. Parsons 500 and 660 MW steam turbines: operating experience and lessons learned. Energy Materials 2009;4:213-37.
[2] Ahmad J, Purbolaksono J, Beng L. Failure analysis on high temperature superheater Inconel® 800 tube. Engineering Failure Analysis 2010;17:328-33.
[3] Ejaz N, Qureshi I, Rizvi S. Creep failure of low pressure turbine blade of an aircraft engine. Engineering Failure Analysis 2011;18:1407-14.
[4] Marriott DL. Isochronous Stress/Strain Curves: Origins, Scope and Applications. ASME 2011 Pressure Vessels and Piping Conference: American Society of Mechanical Engineers Digital Collection; 2011. p. 373-9.
[5] McVetty P. Working stresses for high temperature service. Mech Eng 1934;56:149.
[6] ASME. ASME Boiler & Pressure Vessel Code, Section III Rules for Construction of Nuclear Facility Components, Division 1, Subsection NH, Class 1 Components in Elevated Temperature Service. New York: The American Society of Mechanical Engineers; 2015.
[7] ASME. ASME Boiler & Pressure Vessel Code, Section VIII Rules for Construction of Pressure Vessels Division 2, Alternative Rules. New York: The American Society of Mechanical Engineers; 2015.
[8] Bechtel GS, Cook TS. Load Control–Strain Control Isochronous Stress–Strain Curves for High Temperature Nonlinear Analysis. ASME 1993 International Gas Turbine and Aeroengine Congress and Exposition: American Society of Mechanical Engineers Digital Collection; 1993.
[9] Nadarajah C, Hantz BF, Krishnamurthy S. Using Isochronous Method to Calculate Creep Damage: Part 1. ASME 2017 Pressure Vessels and Piping Conference: American

Society of Mechanical Engineers Digital Collection; 2017.
[10] Xue J, Zhou C, Lu X, Yu X. Plastic limit load of Grade 91 steel pipe containing local wall thinning defect at high temperature. Engineering Failure Analysis 2015;57:171-87.
[11] Zhao M, Koves W. Applications of isochronous data in creep analysis. ASME 2007 Pressure Vessels and Piping Conference: American Society of Mechanical Engineers Digital Collection; 2007. p. 223-30.
[12] Koves W, Zhao M. Comparison of the Isochronous method and a time-explicit model for creep analysis. ASME 2008 Pressure Vessels and Piping Conference: American Society of Mechanical Engineers Digital Collection; 2008. p. 751-9.
[13] Koves W, Zhao M. On Simplified Inelastic Method Using Material's Isochronous Stress–Strain Data for Creep Analysis. Journal of Pressure Vessel Technology 2013;135.
[14] Manu C, Birk A, Kim I. Uniaxial high-temperature creep property predictions made by CDM and MPC omega techniques for ASME SA 455 steel. Engineering Failure Analysis 2009;16:1303-13.
[15] Rouse JP, Sun W, Hyde TH, Morris A. Comparative assessment of several creep damage models for use in life prediction. International Journal of Pressure Vessels and Piping 2013;108-109:81-7.
[16] Wang X-Y, Wang X, Zhang X-C, Zhu S-F. Creep damage characterization of UNS N10003 alloy based on a numerical simulation using the Norton creep law and Kachanov–Rabotnov creep damage model. Nuclear Science and Techniques 2019;30:65.
[17] Pandey VB, Singh IV, Mishra BK. A stress triaxiality based modified Liu–Murakami creep damage model for creep crack growth life prediction in different specimens. International Journal of Fracture 2020;221:101-21.
[18] Haque MS, Stewart CM. Finite-Element Analysis of Waspaloy Using Sinh Creep-Damage Constitutive Model Under Triaxial Stress State. Journal of Pressure Vessel Technology 2016;138.
[19] Prager M. Development of the MPC Omega Method for Life Assessment in the Creep Range. Journal of Pressure Vessel Technology 1995;117:95-103.
[20] Prager M. The Omega Method–An Engineering Approach to Life Assessment. Journal of Pressure Vessel Technology 2000;122:273-80.
[21] Tereda S. Application of Code Case 2605 for Fatigue Evaluation of Vessels Made in 2.25 Cr-1Mo-0.25 V Steels Slightly Into Creep Range. Journal of Pressure Vessel Technology 2013;135.
[22] Vivio F, Gaetani L, Ferracci M, Masia A. Detail investigation of Omega method for creep analysis of pressure vessel components. ASME; 2013.
[23] API. API 579-1/ASME FFS-1, Fitness-For-Service. Houston, TX: American Petroleum Institute; 2016.
[24] ASME. ASME Boiler and Pressure Vessel Code Case 2605-3, Fatigue Evaluation for SA-182 F22V, SA-336 F22V, SA-541 22V, SA-542 Type D, Class 4a, and SA-832 Grade 22V at Temperatures Greater Than 371°C (700°F) and Less Than or Equal to 482°C (900°F) Section VIII, Division 2. New York: American Society of Mechanical Engineers; 2017.
[25] Ainsworth RA e. R5: an assessment procedure for the high temperature response of structures. Procedure R5: Issue 3. Gloucester: UK: British Energy Generation Ltd.; 2014.
[26] Chen H, Engelhardt M, Ponter AR. Linear matching method for creep rupture assessment. International journal of pressure vessels and piping 2003;80:213-20.
[27] Barbera D, Chen H. Creep rupture assessment by a robust creep data interpolation

using the Linear Matching Method. European Journal of Mechanics-A/Solids 2015;54:267-79.
[28] Gorash Y, Chen H. A parametric study on creep–fatigue strength of welded joints using the linear matching method. Int J Fatigue 2013;55:112-25.
[29] Gorash Y, Chen H. On creep-fatigue endurance of TIG-dressed weldments using the linear matching method. Engineering Failure Analysis 2013;34:308-23.
[30] Ponter ARS, Chen H. Modeling of the Behavior of a Welded Joint Subjected to Reverse Bending Moment at High Temperature. Journal of Pressure Vessel Technology 2006;129:254-61.
[31] Chen HF, Ponter ARS. Integrity assessment of a 3D tubeplate using the linear matching method. Part 2: Creep relaxation and reverse plasticity. International Journal of Pressure Vessels and Piping 2005;82:95-104.
[32] PONTER ARS, CHEN H, WILLIS MR, EVANS WJ. Fatigue-creep and plastic collapse of notched bars. Fatigue & Fracture of Engineering Materials & Structures 2004;27:305-18.
[33] Gorash Y, Chen H. Creep-fatigue life assessment of cruciform weldments using the linear matching method. International Journal of Pressure Vessels and Piping 2013;104:1-13.
[34] Kim W-G, Lee H-Y, Hong H-U. Evaluation of tension and creep rupture behaviors of long-term exposed P91 steel in a supercritical plant. Engineering Failure Analysis 2020;116:104736.
[35] Taniguchi G, Yamashita K, Otsu M, Nako H, Sakata M. A study on the development of creep rupture and temper embrittlement properties in 21/4Cr-1Mo-V steel weld metal. Welding in the World 2015;59.
[36] Ure J, Chen H, Tipping D. Verification of the Linear Matching Method for Limit and Shakedown Analysis by Comparison With Experiments. Journal of Pressure Vessel Technology 2015;137.
[37] ASME. ASME Boiler & Pressure Vessel Code, Section II Materials Part D, Properties (Metric). New York: The American Society of Mechanical Engineers; 2015.
[38] Systèmes D. Abaqus 6.12 Abaqus User's Manual. USA2012.
[39] Liu H, Xuan F-Z. A new model of creep rupture data extrapolation based on power processes. Engineering Failure Analysis 2011;18:2324-9.
[40] Gong J-G, Liu F, Xuan F-Z. On fatigue design curves for 2.25 Cr-1Mo-V steel reactors at elevated temperature in Code Case 2605. Journal of Pressure Vessel Technology 2018;140.
[41] Barbera D, Chen H, Liu Y. On Creep Fatigue Interaction of Components at Elevated Temperature. Journal of Pressure Vessel Technology 2016;138.
[42] Giugliano D, Barbera D, Chen H, Cho N-K, Liu Y. Creep-fatigue and cyclically enhanced creep mechanisms in aluminium based metal matrix composites. European Journal of Mechanics - A/Solids 2019;74:66-80.
[43] Chen H, Ponter ARS. A Direct Method on the Evaluation of Ratchet Limit. Journal of Pressure Vessel Technology 2010;132.
[44] Chen H, Chen W, Li T, Ure J. Shakedown Analysis of a Composite Cylinder With a Cross-Hole. Journal of Pressure Vessel Technology 2011;133.
[45] Chen H, Chen W, Ure J. A direct method on the evaluation of cyclic steady state of structures with creep effect. Journal of Pressure Vessel Technology 2014;136.

[46] Bradford R, Ure J, Chen H. The Bree problem with different yield stresses on-load and off-load and application to creep ratcheting. International Journal of Pressure Vessels and Piping 2014;113:32-9.
[47] Marriott DL, Sreeranganathan A, Carter P, Read S. Experience in the Application of the Omega Creep Model in Creep Experiments and Component Analysis. Pressure Technology: American Society of Mechanical Engineers; 2014. p. 151-61.

Appendix A: The calculation process of creep strain rate by Omega model

According to Ref. [19, 20, 24, 47], the creep strain rate needed by equation (5) is able to be calculated through the equations as follows when implementing the creep simulation by coding the ABAQUS user subroutine.

Firstly, in a calculation increment, the original creep rate, $\dot{\varepsilon}_{oc}$, in equation (A 1) is determined by the non-linear creep FEA procedure to produce the results of stress components in equation (A 3).

$$\log_{10}\dot{\varepsilon}_{oc} = -\left\{A_0 + \left(\frac{A_1 + A_2 S_l + A_3 S_l^2 + A_4 S_l^3}{273 + T}\right)\right\} \quad \text{(A 1)}$$

$$S_l = \log_{10}(\sigma_e) \quad \text{(A 2)}$$

$$\sigma_e = \frac{1}{\sqrt{2}}[(\sigma_1 - \sigma_2)^2 + (\sigma_1 - \sigma_3)^2 + (\sigma_2 - \sigma_3)^2]^{0.5} \quad \text{(A 3)}$$

Next, the creep damage rate, $\dot{D}_c$, defined in equation (A 5) is dependent on the Omega parameter, Ω_m, which is given out through equations (A 6) to (A 11). Here A_i and B_i $(i = 1,2,3,4)$ are creep data of strain rate parameters and Omega parameters[24] of 2.25Cr-1Mo-V, and p refers to the hydrostatic stress.

$$D_C = \int_0^t \dot{D}_c dt \leq 1.0 \quad \text{(A 4)}$$

$$\dot{D}_c = \Omega_m \dot{\varepsilon}_{oc} \quad \text{(A 5)}$$

$$\Omega_m = \Omega_n^{\delta+1} \quad \text{(A 6)}$$

$$\Omega_n = \max[(\Omega - n),\ 3.0] \quad \text{(A 7)}$$

$$\log_{10}\ \Omega = B_0 + \left(\frac{B_1 + B_2 S_l + B_3 S_l^2 + B_4 S_l^3}{273 + T}\right) \quad \text{(A 8)}$$

$$n = -\left(\frac{A_2 + 2A_3 S_l + 3A_4 S_l^2}{460 + T}\right) \quad \text{(A 9)}$$

$$\delta = \beta\left(\frac{3p}{\sigma_e} - 1.0\right) \quad \text{(A 10)}$$

$$p = \frac{\sigma_1 + \sigma_2 + \sigma_3}{3} \quad \text{(A 11)}$$

Then in this analysis increment, the net increment of creep damage, D_C, is obtained by integrating the creep damage rate over a time increment, and finally, the creep strain

rate is provided for equation (5) to compute the creep strain.